https://doi.org/10.5194/egusphere-2023-46
Preprint. Discussion started: 24 February 2023

A Novel Eulerian Reaction-Transport Model to Simulate Age and Reactivity Continua Interacting with Mixing Processes

Jurjen Rooze[1], Heewon Jung[2], and Hagen Radtke[1]

[1]Department of Physical Oceanography and Instrumentation, Leibniz Institute for Baltic Sea Research (IOW), Warnemünde, Germany.
[2]Department of Geological Sciences, Chungnam National University, Daejeon, South Korea.

Correspondence: Jurjen Rooze (jurjen.rooze@io-warnemuende.de)

Abstract. In geoscientific models, it can be useful to attribute properties to particles in a continuum. Lagrangian frameworks aim to simulate sufficiently large numbers of individual particles to describe the evolution of the properties and their statistical distributions. Here we present an Eulerian approach: Diffusion-advection-reaction type of partial differential equations are derived for centralized moments, which can describe the distribution of properties associated with chemicals in reaction-transport models. When the property is age, the equations for centralized moments (unlike non-central moments) do not require terms to account for aging, making this method suitable for modeling age tracers. The properties described by the distributions may also affect reaction rates. In practical applications, continuous distributions of ages or reactivities are resolved to simulate organic matter mineralization in surficial sediments, where transport is typically dominated by macrofaunal and physical mixing processes. These applications show the potential of the method to simulate reactivity continua in disturbed environments and reveal practical limitations.

1 Introduction

The partial differential equation (PDE) to describe chemical diffusion (Fick, 1855) is mathematically equivalent to Fourier's heat conduction equation (Fourier et al., 1822), which has become ubiquitous in science to describe random transport processes (Narasimhan, 1999). When material is transported, it can be desirable to track other associated properties besides the concentration. Particularly, age of fluids and chemicals have often been simulated. Diffusive mixing will lead to a local spreading in ages. To resolve the distributions, Langrangian and Eulerian approaches have been developed. The latter have the advantage that they can be analytically evaluated and are computationally less expensive. Analytical solutions for age distributions in particular boundary condition problems can be found in Delhez and Deleersnijder (2002) and Kuderer et al. (2022). Deleersnijder et al. (2001) and Delhez and Deleersnijder (2002) derived Eulerian PDEs to simulate the effect of diffusion on the mean and higher non-central moments and considered the effect of radioactive decay on age distributions. Here we will derive Eulerian PDEs for centralized moments. These are more readily intuitively understood than non-central moments, and they are not affected by aging, making them ideal for modeling time tracers.

Beyond modeling passive tracers, we intend to test moment-based PDEs in more complex applications, whereby reaction rates depend on and affect distributions. Modeling the effect of "aging" on the apparent organic matter reactivity (Middelburg,

https://doi.org/10.5194/egusphere-2023-46
Preprint. Discussion started: 24 February 2023

1989, 2019) provides an interesting practical case study. Bulk organic matter in sediments and soils contains materials with varying reactivities (e.g., De Leeuw and Largeau, 1993), and the bulk degradation rate depends on the entire matrix. As more reactive components disappear first, the remaining organic matter becomes more refractory (Zonneveld et al., 2010). Organic molecules also undergo transformations, which generally lower the reactivity (Burdige, 2007). The overall decreasing reactivity over time is contained in the concept of aging. In multi-G models, separate state variables represent discrete classes of varying reactivities (Jørgensen, 1978; Westrich and Berner, 1984). The reactivity of organic matter may also be described as a continuum for which various distribution functions have been proposed (e.g., Boudreau and Ruddick, 1991; Vähätalo et al., 2010; Xu et al., 2022). The gamma distribution is most commonly used (Arndt et al., 2013; Freitas et al., 2021), in part, because it allows an analytical solution for the evolution of the continuum over time (Boudreau and Ruddick, 1991). It can be easily implemented in sediment models by replacing time with sediment depth based on the assumption of a constant burial velocity or a reconstruction of the deposition history. However, the space-for-time substitution only accounts for the burial of particulate organic matter and ignores mixing processes.

Animals and plants continuously cause disturbances in sediments, which is referred to as bioturbation in literature (Meysman et al., 2006). Bioturbation typically dominates the transport of solids in sediments up to a depth of $\sim$10 cm (Tromp et al., 1995; Middelburg et al., 1997; Boudreau, 1994). In reaction-transport models, this process is most commonly implemented as Fickian transport (Goldberg and Koide, 1962; Guinasso and Schink, 1975; Meysman et al., 2005), i.e., as chemical diffusion, but with a diffusivity decreasing over depth. Mixing of particulate organic matter can also be the result of other natural processes or anthropogenic activities, such as trawl fishing (e.g., De Borger et al., 2021). Previously, Lagrangian methods have been developed to simulate organic matter mineralization in turbated sediments (Meile and Van Cappellen, 2005; Kuderer et al., 2022), but these have only included limited reaction networks with few chemicals. The development of an alternative Eulerian approach, compatible with classical early diagenetic reaction-transport models (Wang and Van Cappellen, 1996; Boudreau, 1997), may be needed to encourage wider usage of modeled reactivity continua in turbated environments.

2 Derivation of partial differential equations for diffusion

Diffusion is a process that mixes distributions of properties associated with moving particles. In the derivation, we will assume that the property of interest is age, even though it could be any other scalar property that does not affect transport. First, we derive equations for chemical diffusion (see 2.1) and the effect of diffusion on mean age (see 2.2) to illustrate the method based on microscopic diffusion. We then derive partial differential equations for higher centralized moments (see 2.3).

2.1 Miscroscopic derivation for concentration

Following Crank (1956), microscopic diffusion can be represented as random jumps forth and back. Consider three locations left (L), center (C), and right (R) aligned on a line and separated by the jumping distance of particles δ_x. The change in the number of molecules at location 'C' is given by

$$\frac{\Delta n_C}{\Delta t} = 0.5 f_r (n_R - n_C) - 0.5 f_l (n_C - n_L) \tag{1}$$

https://doi.org/10.5194/egusphere-2023-46
Preprint. Discussion started: 24 February 2023

where f_x is the jumping frequency in two directions, and n_X is the number of particles at location X. Smaller case and upper case subscripts indicate evaluations at the boundaries and centers of cells, respectively. After dividing by volume V, defining $C = n/V$, and also multiplying the right-hand side by δ_x^2/δ_x^2

$$\frac{\Delta C_C}{\Delta t} = \frac{1}{\delta_x}\left(\frac{0.5 f_r \delta_x^2 (C_R - C_C)}{\delta_x} - \frac{0.5 f_l \delta_x^2 (C_C - C_L)}{\delta_x}\right) \tag{2}$$

is obtained. The diffusivity is identified as $D = 0.5 f \delta_x^2$. One linearization is made, i.e. $\Delta C = \partial C/\partial x \delta_x$, resulting in

$$\frac{\Delta C_C}{\Delta t} = \frac{1}{\delta_x}\left(D_r \left.\frac{\partial C}{\partial x}\right|_r - D_l \left.\frac{\partial C}{\partial x}\right|_l\right) \tag{3}$$

Applying the divergence theorem yields

$$\frac{\partial C}{\partial t} = \frac{\partial}{\partial x}\left(D \frac{\partial C}{\partial x}\right) \tag{4}$$

which is the diffusion equation.

2.2 Microscopic derivation of the diffusion equation for the mean

The same method is applied to the mean age associated with particles, which is the first non-central moment. Let τ_i be the age of a particle and $\sum_{i=1}^{n} \tau_i$ the total age of all particles n in a control volume V, so that the mean age of the particles is $\mu = \sum \tau / n$. Then $\mu C = \sum \tau / V$ is the summed ages of all particles per control volume.

Let j_1 and j_4 be the fluxes that transport particles into the control volume from left and right, respectively. Similarly, let j_2 and j_3 be the fluxes that remove matter in rightward and leftward direction, respectively. Substituting the summed total age of particles for the total number of particles in equation 1 yields

$$\frac{\Delta(C_C \mu_C)}{\Delta t} = \frac{1}{V}\left[j_4 \mu_{j_4} - j_3 \mu_{j_3} - (j_2 \mu_{j_2} - j_1 \mu_{j_1})\right] \tag{5}$$

whereby μ_j are the mean ages of the jumping particles, and the fluxes j_k have dimensions of number of particles over time. Note that this section only considers changes to the local mean age caused by diffusive transport. In section 3, derivations will also account for the effect of aging on the mean. From equation 1 follows that $j_1 = 0.5 f_l n_L$, $j_2 = 0.5 f_l n_C$, $j_3 = 0.5 f_r n_C$, and $j_4 = 0.5 f_r n_R$. When it is assumed that the random jumps are not affected by age, the mean age of a larger number of jumping particles will approach the mean age at the source location X, so that $\langle \mu_{j_k} \rangle = \mu_X$. Making this substitution and repeating the steps that were taken for the derivation of chemical diffusion yields

$$\left\langle \frac{\Delta(C_C \mu_C)}{\Delta t} \right\rangle = \frac{1}{\delta_x}\left(\frac{D_r (C_R \mu_R - C_C \mu_C)}{\delta_x} - \frac{D_l (C_C \mu_C - C_L \mu_L)}{\delta_x}\right) \tag{6}$$

Again a linearizing assumption $\Delta(\mu C) = \partial(\mu C)/\partial x \delta_x$ is made, after which the partial differential equation

$$\frac{\partial (C\mu)}{\partial t} = \frac{\partial}{\partial x}\left(D \frac{\partial (C\mu)}{\partial x}\right) \tag{7}$$

is obtained. Deleersnijder et al. (2001) derived this equation with a generalized macroscopic approach.

https://doi.org/10.5194/egusphere-2023-46
Preprint. Discussion started: 24 February 2023

2.3 Derivation of partial differential equations for higher centralized moments

Centralized moments are defined as

$$\phi = \frac{\sum_{i=1}^{n}(X_i - \mu)^q}{n} \tag{8}$$

The zeroth and first centralized moments are always one and zero, respectively. The variance (σ^2), skewness, and other higher moments correspond to $q = 2$, $q = 3$, and $q > 3$.

Considering the exchange of matter with the surroundings through the fluxes j_k (see section 2.2), the change of q-powered differences in the control volume can be described by

$$\frac{1}{V}\sum_{i=1}^{n_n}(X_i - \mu_o)^q = \frac{1}{V}\sum_{j=1}^{n_o}(X_j - \mu_o)^q + \frac{1}{V}(\phi_{j_1}j_1 - \phi_{j_2}j_2 - \phi_{j_3}j_3 + \phi_{j_4}j_4)\Delta t \tag{9}$$

whereby n_n and n_o denote the number of particles in the updated and old population, respectively. All differences in equation 9, including those associated with mass fluxes, are relative to μ_o. A Taylor series expansion of ϕ around μ_o is used to relate the new state of a population (the left-hand side of equation 9) to the new mean age

$$\frac{1}{V}\sum_{i=1}^{n_n}(X_i - \mu_n)^q = \frac{1}{V}\sum_{i=1}^{n_n}(X_i - \mu_o)^q + C_n\phi'\Delta\mu + C_n\frac{\phi''}{2}\Delta\mu^2 + C_n\frac{\phi'''}{6}\Delta\mu^3 + \ldots \tag{10}$$

where $C_n = n_n/V$, $\Delta\mu = \mu_n - \mu_o$, and $\phi' = \partial\phi/\partial\mu$, etc. The term on the left-hand side of equation 10 and the first on the right hand-side of equation 9 can be replaced by $C_n\phi_n$ and $C_o\phi_o$, respectively. By inserting equation 10 into equation 9 and rearranging the terms, the expression

$$C_n\phi_n - C_o\phi_o - C_n\phi'\Delta\mu - C_n\frac{\phi''}{2}\Delta\mu^2 - C_n\frac{\phi'''}{6}\Delta\mu^3 - \ldots = \frac{1}{V}(\sum_{k=1}^{4}\lambda_k\phi_{j_k}j_k)\Delta t \tag{11}$$

is obtained, whereby $\lambda_k = \pm 1$ depending on the direction of the flux.

2.3.1 Derivation of a partial equation for variance

The derivatives of variance in the Taylor series are

$$\frac{\partial\sigma^2}{\partial\mu} = -2\frac{\sum(X_i - \mu)}{n} = 0 \tag{12a}$$

$$\frac{\partial^2\sigma^2}{\partial\mu^2} = 2 \tag{12b}$$

$$\frac{\partial^3\sigma^2}{\partial\mu^3} = 0 \tag{12c}$$

The only non-zero derivative is inserted into equation 11. The linearization $\Delta\mu = \partial\mu/\partial t\Delta t$ is made, and the result is divided by Δt. Taking the limit of Δt to zero yields

$$\lim_{\Delta t\to 0}\left[\frac{C_n\sigma_n^2 - C_o\sigma_o^2}{\Delta t} - C_n\left(\frac{\partial\mu}{\partial t}\right)^2\Delta t\right] = \frac{1}{V}\sum_{k=1}^{4}\lambda_k\sigma_{j_k}^2 j_k \tag{13}$$

https://doi.org/10.5194/egusphere-2023-46
Preprint. Discussion started: 24 February 2023

Table 1. Partial differentials equation for diffusion of concentration, mean, and centralized moments.

Moment	Variable	Diffusion equation
Concentration	C	$\frac{\partial C}{\partial t} = \frac{\partial}{\partial x}\left(D\frac{\partial C}{\partial x}\right)$
Mean	μ	$\frac{\partial (C\mu)}{\partial t} = \frac{\partial}{\partial x}\left(D\frac{\partial (C\mu)}{\partial x}\right)$
Variance	$\phi_2 = \sigma^2$	$\frac{\partial (C\sigma^2)}{\partial t} = \frac{\partial}{\partial x}\left(D\frac{\partial (C\sigma^2)}{\partial x}\right) + 2DC\left(\frac{\partial \mu}{\partial x}\right)^2$
Higher moments	ϕ_q	$\frac{\partial (C\phi_q)}{\partial t} = \frac{\partial}{\partial x}\left(D\frac{\partial (C\phi_q)}{\partial x}\right) + 2qDC\frac{\partial \phi_{q-1}}{\partial x}\frac{\partial \mu}{\partial x}$

See for the definition of the centralized moments (ϕ_q) equation 8.

or, under the assumption that $\partial\mu/\partial t$ is finite,

$$\frac{\partial (C\sigma^2)}{\partial t} = \frac{1}{V}\sum_{k=1}^{4} \lambda_k \sigma_{j_k}^2 j_k \tag{14}$$

in differential form.

In the next step, the unknown fluxes on the right-hand side are expressed by known local properties, which can only be done for expected mean values of a large number of random particle jumps. It will be assumed for the partial differential equation for variance, as well as for higher order moments, that i) the flux is determined by the average jumping frequency and the number of particles from a source location X, i.e. $j_k = f n_X$, ii) that q-powered differences reflect the average differences from the location where the particles are jumping, i.e. $\phi_{j_k} = \phi_X$, and iii) that the properties of particles do not effect the jumping probability, i.e. $\langle j_k \phi_{j_k} \rangle = \langle j_k \rangle \langle \phi_{j_k} \rangle$.

With these assumptions, one can write

$$\left\langle \frac{1}{V}\sum_{k=1}^{4} \lambda_k \sigma_{j_k}^2 j_k \right\rangle = \frac{f_r}{2}\left[\sigma_R^2(\mu_C)C_R - \sigma_C^2(\mu_C)C_C\right] - \frac{f_l}{2}\left[\sigma_C^2(\mu_C)C_C - \sigma_L^2(\mu_C)C_L\right] \tag{15}$$

Using the Taylor series for spatial instead of temporal derivatives, i.e. $\Delta\mu = \mu_R - \mu_C$ or $\mu_C - \mu_L$, gives according to equations 12a - 12c

$$\sigma_L^2(\mu_C) = \sigma_L^2(\mu_L) + (\mu_C - \mu_L)^2 \tag{16a}$$

$$\sigma_R^2(\mu_C) = \sigma_R^2(\mu_R) + (\mu_C - \mu_R)^2 \tag{16b}$$

and substituting these into equation 15 yields

$$\begin{aligned} \left\langle \frac{1}{V}\sum_{k=1}^{4} \lambda_k \sigma_{j_k}^2 j_k \right\rangle \quad = \quad & \frac{f_r}{2}\left[(\sigma_R^2(\mu_R) + (\mu_C - \mu_R)^2)C_R - \sigma_C^2(\mu_C)C_C\right] - \\ & \frac{f_l}{2}\left[\sigma_C^2(\mu_C)C_C - (\sigma_L^2(\mu_L) + (\mu_C - \mu_L)^2)C_L\right] \end{aligned} \tag{17}$$

https://doi.org/10.5194/egusphere-2023-46
Preprint. Discussion started: 24 February 2023

Ignoring the terms with derivatives obtained from the Taylor series for the moment, a part of the equation can be isolated

$$\left\langle \frac{1}{V}\sum_{k=1}^{4}\lambda_k\sigma_{j_k}^2 j_k \right\rangle^{*} = \frac{f_r}{2}\left[\sigma_R^2(\mu_R)C_R - \sigma_C^2(\mu_C)C_C\right] - \frac{f_l}{2}\left[\sigma_C^2(\mu_C)C_C - \sigma_L^2(\mu_L)C_L\right] \tag{18}$$

which is similar to equation 5. A linearization of $\partial(\sigma^2 C)/\partial x$ and repeating the procedure leading from equation 5 to equation 7 gives here

$$\left\langle \frac{1}{V}\sum_{k=1}^{4}\lambda_k\sigma_{j_k}^2 j_k \right\rangle^{*} = \frac{\partial}{\partial x}\left(D\frac{\partial(C\sigma^2)}{\partial x}\right) \tag{19}$$

The remaining terms not accounted for yet are

$$\left\langle \frac{1}{V}\sum_{k=1}^{4}\lambda_k\sigma_{j_k}^2 j_k \right\rangle^{**} = \frac{f_r}{2}(\mu_C-\mu_R)^2 C_R + \frac{f_l}{2}(\mu_C-\mu_L)^2 C_L \tag{20}$$

which can also be written as

$$\left\langle \frac{1}{V}\sum_{k=1}^{4}\lambda_k\sigma_{j_k}^2 j_k \right\rangle^{**} = \frac{D_r}{\delta_x^2}\left(\frac{\partial\mu}{\partial x}\delta_x\right)^2 C_R + \frac{D_l}{\delta_x^2}\left(\frac{\partial\mu}{\partial x}\delta_x\right)^2 C_L \tag{21}$$

yielding in the limit of $\Delta x \to 0$

$$\left\langle \frac{1}{V}\sum_{k=1}^{4}\lambda_k\sigma_{j_k}^2 j_k \right\rangle^{**} = 2DC\left(\frac{\partial\mu}{\partial x}\right)^2 \tag{22}$$

Therefore,

$$\frac{\partial(C\sigma^2)}{\partial x} = \frac{\partial}{\partial x}\left(D\frac{\partial(C\sigma^2)}{\partial x}\right) + 2DC\left(\frac{\partial\mu}{\partial x}\right)^2 \tag{23}$$

is the final result describing the effect of diffusion on the centralized variance. The PDE for diffusion of the non-central variance (not shown) can be derived from equation 23 and matches with the result of Delhez and Deleersnijder (2002), which shows that the additional linearizations made in the derivation do not affect the accuracy.

2.3.2 Derivation of partial equations for skewness and all higher order moments

In equation 11, we divide by an infinitesimally small time step. For a finite $\partial\mu/\partial t$, this implies that the higher-order terms in the Taylor series drop, leaving

$$\frac{\partial(C\phi)}{\partial t} - C\phi'\frac{\partial\mu}{\partial t} = \frac{1}{V}\sum_{k=1}^{4}\lambda_k\phi_{j_k}j_k \tag{24}$$

The presence of a non-zero first-order derivative makes the derivation of the PDEs for higher-order moments different from that of the variance. It can be found in appendix A. An overview of all PDEs for diffusion is shown in Table 1.

https://doi.org/10.5194/egusphere-2023-46
Preprint. Discussion started: 24 February 2023

3 Applications

Three applications related to sedimentary environments are presented. For the sake of simplicity and generality, the effect of sediment properties, such as porosity and tortuosity, on transport will be ignored. Instead, the focus is on adding reaction terms.

3.1 Simulating an age tracer

In sediment modeling, resolving the age of a chemical compound, understood as the time since its formation or deposition onto the sediment, can help to fit a measured profile. For instance, it allows to relate the presence of peaks and troughs in a solid profile, such as the concentration of particulate organic carbon over depth, to changes in the depositional history.

A general system of equations for an age associated with a chemical concentration C is given by

$$\frac{\partial C}{\partial t} = J_0 - \frac{\partial(\omega C)}{\partial x} + R_1 - R_2 \tag{25a}$$

$$\frac{\partial(C\mu)}{\partial t} = J_1 - \frac{\partial(\omega C\mu)}{\partial x} + C - \mu R_2 \tag{25b}$$

$$\frac{\partial(C\phi_q)}{\partial t} = J_q - \frac{\partial(\omega C\phi_q)}{\partial x} + R_1^{\phi_q} - \phi_q R_2 \tag{25c}$$

In the equations, J denotes the diffusive transport terms listed in Table 1. The second term accounts for advective transport, whereby ω is the velocity. In early diagenetic models, the accumulation of the sediment column is typically described as a downward advective burial process, since the sediment surface stays at a zero vertical coordinate.

The terms R_1 and R_2 represent formation and consumption reactions, respectively. The third term in equation 25b accounts for aging ($\partial(C\mu)/\partial t|_A = C\partial\mu/\partial t = C$). New material produced by R_1 has an age of zero. Since R_1 increases the concentration and does not affect the total age ($C\mu$), it decreases the mean age. Consumption is assumed not to discriminate with respect to the age of reactants. Therefore, the last term in equation 25b affects only the total and not the mean age.

The effect of reactions on higher moments (e.g., $R_1^{\phi_q}$ in equation 25c) can be derived from the definition in equation 8, to which the binomial theorem is applied,

$$C\phi_q = \sum_{j=0}^{q}\left[\binom{q}{j}(-\mu)^j \sum_{i=1}^{n}(\tau_i^{q-j})\right] \tag{26}$$

Taking the derivative with respect to time yields in continuous form

$$\frac{\partial(C\phi_q)}{\partial t} = \sum_{j=0}^{q}\left\{(-1)^j\binom{q}{j}\left[\mu^j\frac{\partial(C\mu_{q-j})}{\partial t} + \frac{\partial\mu^j}{\partial t}C\mu_{q-j}\right]\right\} \tag{27}$$

whereby $\mu_x = C^{-1}\int \tau^x C_\tau\, d\tau$ is identified as the x-th non-central moment. When no subscript is given, $\mu = \mu_1$ denotes the mean. Centralized moments (ϕ_k) are transformed to non-central moments (μ_x) by

$$\mu_x = C\sum_{k=0}^{x}\binom{x}{k}\phi_k\mu^{x-k} \tag{28}$$

https://doi.org/10.5194/egusphere-2023-46
Preprint. Discussion started: 24 February 2023

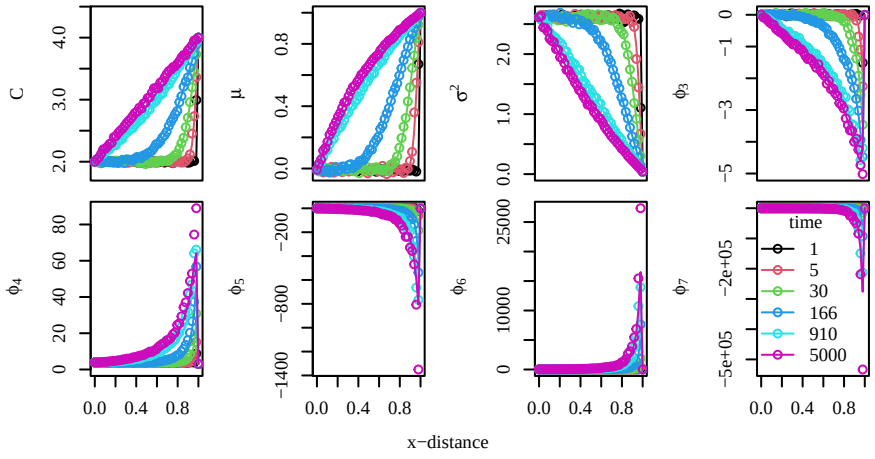

Figure 1. Profiles of moments evolving over time due to diffusion. Solution of numerical integration of partial differential equations (solid lines) is compared to a particle tracking simulation (circles). Domain contains 50 cells. The spacing and time steps are set equal to the jumping distance and the inverse jumping frequency of particles, respectively.

The temporal derivative of μ^j can be expressed as

$$\frac{\partial \mu^j}{\partial t} = j\mu^{j-1}\frac{\partial \mu}{\partial t} \tag{29}$$

Considering the product rule $\partial\mu/\partial t = [\partial(\mu C)/\partial t - \mu\partial C/\partial t]/C$, the effect of the reaction on the mean is $\partial\mu/\partial t = -\mu R_1/C$. For the production of new material, the temporal derivatives of $C\mu_x$ are zero. Inserting these terms into equation 27 yields $R_1^{\phi_q}$. The expression for R_2 in equation 25c can be more readily obtained by verifying that consumption should not affect the higher centralized moments.

An example of a simulation involving diffusion without aging, advection, and reactions is shown in Figure 1. Here fixed concentrations and moments were imposed for the last and first cells in the domain as boundary conditions. The initial conditions for the domain were set to the left boundary condition, which has a lower concentration and different moments compared to the right boundary. Over time, there is net chemical diffusion in the leftward direction throughout the domain, eventually leading to a new steady state. The Eulerian simulation is based on a finite differences scheme, implemented in R (R Core Team, 2022) and run with the CVODE solver (Brown et al., 1989; Soetaert et al., 2010). The computed concentration and the first seven moments match well with those computed by a particle-based simulation. There is a small but noticeable mismatch at the peak for the skewness and higher moments, which is potentially due to the finite step size in the Lagrangian simulation. The script to run these simulations is relatively simple and publicly available online. Therein, it is possible to add reactions for production and consumption.

https://doi.org/10.5194/egusphere-2023-46
Preprint. Discussion started: 24 February 2023

3.2 Simulating organic matter mineralization with a reactivity continuum model in turbated sediments

In this application, C denotes organic carbon concentration, $\tau = k$ is a reactivity (degradation rate coefficient) with dimensions T^{-1}, and there is no explicit aging term. As an example, we will consider an initially uniform distribution for $k \in [0, m]$, which is described by the state variables concentration, mean reactivity, and variance of the reactivity.

Considering all reactive particle, the rate can be expressed as $R = \sum k_i C_i = \bar{k} C$. Then

$$\frac{\partial C}{\partial t}|_R = \bar{k} C \tag{30a}$$

$$\frac{\partial (C\mu)}{\partial t}|_R = \int_0^m (k^2 C)\, dk \tag{30b}$$

$$\frac{\partial (C\sigma^2)}{\partial t}|_R = \int_0^m (k^3 C)\, dk - 2\bar{k} \int_0^m (k^2 C)\, dk + \bar{k}^3 C \tag{30c}$$

become the equations describing the effect of the reactions on the moments.

The integrals will be evaluated numerically, meaning that the full distribution needs to be constructed from the moments. Based on a finite number of moments, it can only be estimated, and we chose the function

$$g(k, \boldsymbol{w}) = C_0 e^{w_0 \sqrt{k} + w_1 k} + w_2 k e^k \tag{31}$$

to represent the reactivity distribution. It is motivated as follows: The concentration of unreactive organic matter at the intercept does not change ($g(0, \boldsymbol{w}) = C_0$). For the diffusion-reaction equation $\partial C/\partial t = D\partial^2 C/\partial x^2 - kC$, the general solution is $Ae^{\pm\sqrt{k/D}x}$. The solution for $\partial C/\partial t = -kC$ is $C(t) = Ae^{-kt}$. The first term can capture both these dynamics. The last term is linearly independent and introduces a third fitting parameter to match the number of equations. These terms have the desirable properties that they cannot fluctuate or become negative and can be evaluated at $k = 0$. To fit the parameter vectors $\boldsymbol{w}$, the equations

$$C - \int_0^m g(k, \boldsymbol{w})\, dk = 0 \tag{32a}$$

$$\mu - \int_0^m g(k, \boldsymbol{w}) k\, dk = 0 \tag{32b}$$

$$\sigma^2 - \int_0^m (k - \bar{k})^2 g(k, \boldsymbol{w})\, dk = 0 \tag{32c}$$

are solved with a multidimensional root-finding procedure (Soetaert, 2009).

In the example shown in Figure 2, transport involves bioturbation and advection. The burial velocity was set to 1 $\mathrm{mm\,y^{-1}}$. The bioturbation coefficient had a maximum value of 10^{-10} $\mathrm{m^2\,s^{-1}}$ at the sediment-water interface and decreased exponentially over depth with an e-folding distance set to 2 cm. Using finite differences (Soetaert and Meysman, 2012), the domain

https://doi.org/10.5194/egusphere-2023-46
Preprint. Discussion started: 24 February 2023

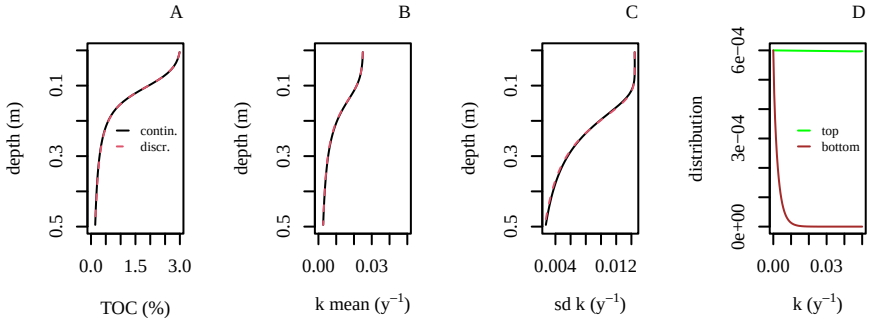

Figure 2. A simulated reactivity continuum (black line) from a simulation run to steady state validated with a discrete 30-G model (dashed red line). Panels A, B, and C show the total organic carbon (TOC) concentration, the mean reactivity, and standard deviation, respectively; panel D shows the distribution function for reactivities at the top (green) and bottom (red) of the model domain.

consisting of 50 evenly spaced cells and having a total domain length of 50 cm was discretized, and the simulation was run with the VODE solver (Brown et al., 1989).

The TOC concentration imposed to a fixed value at the upper boundary condition decreases due to degradation over depth (Figure 2A). The mean reactivity of organic matter remains relatively constant in the top due to mixing, but decreases strongly over depth below the bioturbated zone (Figure 2B), as the more reactive TOC is degraded. The variance is also kept relatively stable within the bioturbated zone, and decreases strongly below (Figure 2C), as the removal of more reactive material decreases the spreading of the reactivity distribution. The distributions at the top and bottom are shown as well (Figure 2D). In this simulation, a no-gradient condition was imposed as the lower boundary condition. The results closely match the results of a discrete 30-G model. The script for these simulations is made publicly available online.

3.3 Apparent organic matter reactivity as a function of age

In this application, the age distribution is modeled and the reactivity of organic carbon depends on the age property. The transport equations are the same as in the previous applications, and aging is turned on (see eq. 25b). Considering $k = f(\tau)$, one can write in continuous form

$$\frac{dC}{dt} = R = \int_a^b f(\tau) C \, d\tau \tag{33}$$

The temporal derivative of the total age due to the removal of material is

$$\frac{\partial(C\mu)}{\partial t}|_R = \int_a^b \tau f(\tau) C \, d\tau \tag{34}$$

https://doi.org/10.5194/egusphere-2023-46
Preprint. Discussion started: 24 February 2023

To derive the temporal derivative of higher centralized moments, the same approach is followed as for the production reaction in the first application. Starting from equation 27, the term

$$\frac{\partial(C\mu_{q-j})}{\partial t}|_R = \int_a^b \tau^{q-j} f(\tau) C \, d\tau \tag{35}$$

is non-zero here. The other term in equation 27 (corresponding to eq. 29) can be found by solving $\partial\mu/\partial t$ from equations 33 and 34.

The age-dependent reaction rate is specified as

$$f(\tau) = \frac{v}{\alpha + \tau} \tag{36}$$

whereby α is set to a small value (10^{-3}) to prevent division by zero. It resembles the expression for the mean reactivity, $\bar{k} = v/(\alpha+\tau)^q$, used by Middelburg (1989). Conceptually it may be the most simple expression to model the effect of aging on reactivity.

The distribution function to fit the moments is defined as

$$g(\tau, \boldsymbol{w}) = \frac{w_2 e^{-w_1 q}}{(1+e^{-w_1 q})^2}\theta(-q) + \frac{w_2 e^{-w_2 q}}{(1+e^{-w_2 q})^2}\theta(q) \tag{37}$$

whereby $q = x - w_3$ and θ is the Heaviside step function. It has a single maximum at $q = 0$ and asymmetric slopes at both sides defined by w_1 and w_2 (see, for example, the dashed curves in Figure 4A). The parameter vector is found by calculating

$$\mu - \int_a^b k g(\tau, \boldsymbol{w}) \, d\tau = \epsilon_1 \tag{38a}$$

$$\sigma^2 - \int_a^b (\tau - \mu)^2 g(\tau, \boldsymbol{w}) \, d\tau = \epsilon_2 \tag{38b}$$

$$S - \int_a^b (\tau - \mu)^3 g(\tau, \boldsymbol{w}) \, d\tau = \epsilon_3 \tag{38c}$$

and minimizing

$$\epsilon_T = \frac{\epsilon_1}{\sqrt{\mu}} + \frac{\epsilon_2}{\sigma^2} + \frac{\epsilon_3}{S^{3/2}} \tag{39}$$

as a weighted fitting cost function. This minimization was used instead of a Jacobian root-finding procedure (see previous application, section 3.2), because the gradient search in the latter procedure failed. After the moments are fitted, the concentration of the distribution is corrected by a multiplication factor. The cumulative distribution function for integrating concentration and equation 38a are analytically solved. The other integrals are numerically evaluated. These require bounds corresponding to the age interval wherein concentrations are significant (the threshold was set to 10^{-9} of the function maximum), and this was also numerically determined.

https://doi.org/10.5194/egusphere-2023-46
Preprint. Discussion started: 24 February 2023

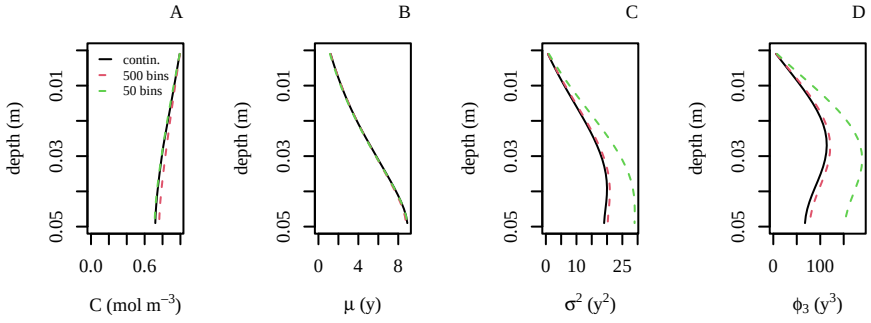

Figure 3. A simulation (black line) with reactivities based on age distributions compared to discrete simulations with 500 (dashed red lines) and 50 (dashed green lines) age bins. Panels A to D show the simulated concentration, mean age, age variance, and age skewness, respectively.

For the simulation shown in Figure 3, the burial velocity was set to 1 $\mathrm{mm\,y^{-1}}$. The bioturbation coefficient had a maximum value of 10^{-11} $\mathrm{m^2\,s^{-1}}$ at the top and decreased exponentially with depth, having an e-folding distance set to 2 cm. Using a finite differences scheme, the simulation was run with the VODE solver (Brown et al., 1989; Soetaert and Meysman, 2012). A grid consisting of 25 cells represented a domain length of 5 cm.

The simulated continuous age distribution (solid black line, Figure 3) is compared to discrete simulations with 500 and 50 discrete age bins (dashed red and green lines, respectively), covering ages between 0 and 60 years. The simulation with 500 discrete classes, validates the simulated mean, variance, and skewness (Figure 3B,C,D). There is a discernible mismatch in the simulated concentration (Figure 3A). This is possibly due to round-off errors in the simulation with 500 age bins, as the simulation with 50 age bins validates the concentration profile from the continuous simulation. As age distributions could not be perfectly reconstructed from the moments (see discussion), the match between the continuous and discrete simulations is surprisingly good.

4 Discussion

The theory outlined in this paper gives modelers a free hand to simulate properties associated with particles described as a concentration. Modelers can use different reaction kinetics and simulate the effect on a continuous distribution. The first application shows that it is possible to reliably simulate numerous moments of an age distribution. In this type of application, it is unnecessary to reconstruct the distribution function from its moments during the simulation. In principle, any distribution is uniquely defined by a large or infinite number of moments. However, in practice, there does not exist a universal solution to retrieve distributions from their moments. Numerical methods have been developed for this purpose (e.g., John et al., 2007; Arbel et al., 2016) but do not always succeed.

In the two other applications, the shape of the distribution affected the reaction rates and, therefore, needed to be resolved in the simulations. For the reactivity continuum model, the shape could be well predicted, i.e. the chosen class of distribution

https://doi.org/10.5194/egusphere-2023-46
Preprint. Discussion started: 24 February 2023

function was a good approximation of the exact solutions. The bounds of the initial distribution of deposited material also provided bounds for the numerical integration of deeper (older) material, since the domain only becomes smaller as the more reactive materials are consumed and the refractory organics remain. These simulations were stable and ran relatively fast, despite the requirement to determine the parameters of the distribution in run-time, which involves several numerical integrations. This approach could be attractive to replace the multi-G approach, as it does not require the somewhat arbitrary definition of various reactivity classes (Jørgensen, 1978). However, the multi-G simulation will still run faster. The initial uniform distribution used in the simulation may not be realistic for organic matter in marine sediment (Boudreau and Ruddick, 1991), but instead, distributions similar to discrete multi-G or continuous distributions found in the literature (Arndt et al., 2013) can be imposed for freshly deposited organics.

The third application was the most challenging, as the shape of the age distribution strongly changed. The bounds of the distribution function needed to be numerically evaluated during run time. Since the age distributions are strongly asymmetric, it was necessary to add skewness as a state variable. The simulations were rather time-consuming, and therefore critical parts were coded in C. The multidimensional root-finding procedure failed. Finding a satisfying fitting cost function (e.g., eq. 39) for a minimization procedure proved to be difficult.

During testing, refitting known distributions based on their moments occasionally gave unsatisfactory results. For example, two fits are shown for a known distribution in Figure 4. The curve that was directly fitted to the actual distribution by minimizing the summed residual errors may appear to reproduce the distribution better than the fit obtained from a reconstruction of the moments. However, the moments of this directly fitted curve are more off than those of the moments-based fit. The cumulative distribution function of the moments-based fit appears to be better, which is important, as the evaluations of the distribution for error minimization involve integrations. A fundamental problem of reconstructing distributions from moments is the unequal weights for concentration differences at different locations on the age/reactivity axis. For central moments, the weight of the fit at $\tau = \mu$ will be zero (see eq. 8), and the weights are highest at the extremes of the distribution. When the fits are imperfect, this will likely introduce biases.

Numerous optimizations can be considered to improve the numerical scheme. Better minimization procedures may be developed. Other polynomial type or spline expressions could be tried to describe the distributions. Finally, pre-calculated search tables for distribution functions could be designed to look up parameters corresponding to a combination of moments. Then numerical integrations during run-time would become obsolete, making simulations faster and potentially more stable.

Code availability. The scripts for the applications are available at https://git.io-warnemuende.de/rooze/DiffussionCentralMoments/src/tag/1.0.

https://doi.org/10.5194/egusphere-2023-46
Preprint. Discussion started: 24 February 2023

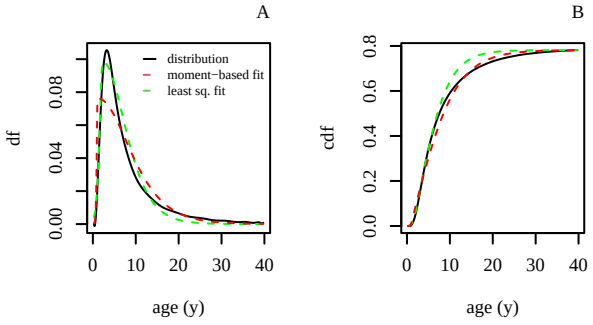

Figure 4. A hypothetical age distribution (black line) is refitted by a reconstruction based on the moments (red dashed line) and a direct fit (green dashed line). The distribution function (df, eq. 37) and cumulative distribution (cdf) functions are shown in panels A and B, respectively. The relative errors in the mean, variance, and skewness of the moments-based fit are 0.0%, 21%, 50%, and those for the direct fit are 16%, 58%, and 80%, respectively.

Appendix A: Derivation of diffusion PDEs for higher centralized moments

Continuing the derivation of the PDE for the diffusion of higher moments from equation 24, one can write

$$\frac{1}{V}\left\langle \sum \lambda_k \phi_{j_k} j_k \right\rangle = -\frac{f_l}{2}\left[\phi_C(\mu_C)C_C - \phi_L(\mu_C)C_L\right] + \frac{f_r}{2}\left[\phi_R(\mu_C)C_R - \phi_C(\mu_C)C_C\right] \tag{A1}$$

when the same assumptions are made with regard to the fluxes as in the derivation for the PDE of the variance. The fluxes j_1 and j_4, transporting material into the control volume, can be written as functions of the mean age at the source location,

$$\phi_L(\mu_L) = \phi_L(\mu_C) + \phi' \cdot (\mu_L - \mu_C) + 0.5\phi'' \cdot (\mu_L - \mu_C)^2 + \ldots \tag{A2a}$$

$$\phi_R(\mu_R) = \phi_R(\mu_C) + \phi' \cdot (\mu_R - \mu_C) + 0.5\phi'' \cdot (\mu_R - \mu_C)^2 + \ldots \tag{A2b}$$

Inserting these equations into equation A1, the part not accounting for the derivatives of the Taylor series is isolated

$$\frac{1}{V}\left\langle \sum \lambda_k \phi_{j_k} j_k \right\rangle^* = \frac{\partial}{\partial x}\left(D\frac{\partial(C\phi)}{\partial x}\right) \tag{A3}$$

whereby $\partial(C\phi)/\partial x$ has been linearized. The terms for the derivatives can be written as

$$\begin{aligned}\frac{1}{V}\left\langle \sum \lambda_k \phi_{j_k} j_k \right\rangle^{**} \quad = \quad & -\frac{f_l C_L}{2}\left(\frac{\partial\phi}{\partial\mu}_L(\mu_L - \mu_C) + \frac{1}{2}\frac{\partial^2\phi}{\partial\mu^2}_L(\mu_L - \mu_C)^2 + \ldots\right) - \\ & \frac{f_r C_R}{2}\left(\frac{\partial\phi}{\partial\mu}_R(\mu_R - \mu_C) + \frac{1}{2}\frac{\partial^2\phi}{\partial\mu^2}_R(\mu_R - \mu_C)^2 + \ldots\right)\end{aligned} \tag{A4}$$

Substituting this and $f/2 = D/\delta_x^2$ into the last equation yields

$$\frac{1}{V}\left\langle \sum \lambda_k \phi_{j_k} j_k \right\rangle^{**} = \frac{D_l C_L}{\delta_x}\left(\frac{\partial\phi}{\partial\mu}_L \frac{\Delta\mu}{\delta_x}_l - \frac{1}{2}\frac{\partial^2\phi}{\partial\mu^2}_L \frac{(\Delta\mu)^2}{\delta_x}_l + \ldots\right) - \frac{D_r C_R}{\delta_x}\left(\frac{\partial\phi}{\partial\mu}_R \frac{\Delta\mu}{\delta_x}_r + \frac{1}{2}\frac{\partial^2\phi}{\partial\mu^2}_R \frac{(\Delta\mu)^2}{\delta_x}_r + \ldots\right) \tag{A5}$$

https://doi.org/10.5194/egusphere-2023-46
Preprint. Discussion started: 24 February 2023

whereby $\mu_C - \mu_L = \Delta\mu_l$ and $\mu_R - \mu_C = \Delta\mu_r$. Taking the limit of Δx to zero, the second-order Taylor series terms will drop. Linearizing $\partial\mu/\partial x$ yields

$$\frac{1}{V}\left\langle \sum \lambda_k \phi_{j_k} j_k \right\rangle^{**} = \frac{D_l C_L}{\delta_x} \frac{\partial \phi}{\partial \mu}_L \frac{\partial \mu}{\partial x}_l - \frac{D_r C_R}{\delta_x} \frac{\partial \phi}{\partial \mu}_R \frac{\partial \mu}{\partial x}_r \tag{A6}$$

Inserting the linearizations

$$\frac{\partial \phi}{\partial \mu}_L = \frac{\partial \phi}{\partial \mu}_C - \frac{\partial^2 \phi}{\partial \mu \partial x}_C \delta_x \tag{A7a}$$

$$\frac{\partial \phi}{\partial \mu}_R = \frac{\partial \phi}{\partial \mu}_C + \frac{\partial^2 \phi}{\partial \mu \partial x}_C \delta_x \tag{A7b}$$

into equation A6 gives

$$\frac{1}{V}\left\langle \sum \lambda_k \phi_{j_k} j_k \right\rangle^{**} = \frac{\partial \phi}{\partial \mu}\left(\frac{D_l C_L}{\delta_x} \frac{\partial \mu}{\partial x}_l - \frac{D_r C_R}{\delta_x} \frac{\partial \mu}{\partial x}_r \right) - 2DC \frac{\partial}{\partial x}\left(\frac{\partial \phi}{\partial \mu} \right) \frac{\partial \mu}{\partial x} \tag{A8}$$

The concentration gradient is also linearized

$$C_L = C_l - \frac{1}{2}\frac{\partial C}{\partial x}\delta_x \tag{A9a}$$

$$C_R = C_r + \frac{1}{2}\frac{\partial C}{\partial x}\delta_x \tag{A9b}$$

When these expressions are inserted and the divergence theorem is applied, the following partial differential equation

$$\frac{1}{V}\left\langle \sum \lambda_k \phi_{j_k} j_k \right\rangle^{**} = -\frac{\partial \phi}{\partial \mu}\left[\frac{\partial}{\partial x}\left(DC \frac{\partial \mu}{\partial x} \right) + D \frac{\partial C}{\partial x}\frac{\partial \mu}{\partial x} \right] - 2DC \frac{\partial}{\partial x}\left(\frac{\partial \phi}{\partial \mu} \right) \frac{\partial \mu}{\partial x} \tag{A10}$$

is obtained.

Finally, it can be shown that the second term on the left-hand side of equation 24 will cancel out with the first term on the right-hand side of equation A10. The time-derivative in equation 24 can be expanded

$$C\frac{\partial \mu}{\partial t} = \frac{\partial}{\partial x}\left(D \frac{\partial (C\mu)}{\partial x} \right) - \mu \frac{\partial}{\partial x}\left(D \frac{\partial C}{\partial x} \right) \tag{A11}$$

Since the concentration gradient was linearized, it can be taken outside the spatial derivative. By applying the product rules several times, the expression

$$C\frac{\partial \mu}{\partial t} = \frac{\partial}{\partial x}\left(DC \frac{\partial \mu}{\partial x} \right) + D \frac{\partial \mu}{\partial x}\frac{\partial C}{\partial x} \tag{A12}$$

can be obtained. The last equation will cancel out with the part between square brackets in equation A10 when it is inserted into equation 24. Inserting the sum of equations A3 and A10 in the right-hand side of equation 24 will yield

$$\frac{\partial (C\phi)}{\partial t} = \frac{\partial}{\partial x}\left(D \frac{\partial (C\phi)}{\partial x} \right) - 2DC \frac{\partial}{\partial x}\left(\frac{\partial \phi}{\partial \mu} \right) \frac{\partial \mu}{\partial x} \tag{A13}$$

Finally, by substituting

$$\frac{\partial \phi_q}{\partial \mu} = -q\phi_{q-1} \tag{A14}$$

the final result shown in Table 1 is derived.

https://doi.org/10.5194/egusphere-2023-46
Preprint. Discussion started: 24 February 2023

Author contributions. J.R. designed the study, derived the equations, wrote the scripts, and performed the research with H.J. and H.R. All authors discussed the results and commented on the manuscript.

Competing interests. The authors declare that they have no competing interests.

Acknowledgements. This work was conducted within the DAM pilot mission "MGF-Ostsee" (Grant No. 03F0848A) funded by the German Federal Ministry of Education and Research. Heewon Jung was supported by the National Research Foundation of Korea (NRF) grant funded by the Korea government (MSIT) (No. 2022R1C1C1004512).

https://doi.org/10.5194/egusphere-2023-46
Preprint. Discussion started: 24 February 2023

References

Arbel, J., Lijoi, A., and Nipoti, B.: Full Bayesian inference with hazard mixture models, Computational Statistics & Data Analysis, 93, 359–372, https://doi.org/10.1016/j.csda.2014.12.003, 2016.

Arndt, S., Jørgensen, B. B., LaRowe, D. E., Middelburg, J., Pancost, R., and Regnier, P.: Quantifying the degradation of organic matter in marine sediments: A review and synthesis, Earth-Science Reviews, 123, 53–86, https://doi.org/10.1016/j.earscirev.2013.02.008, 2013.

Boudreau, B. P.: Is burial velocity a master parameter for bioturbation?, Geochimica et Cosmochimica Acta, 58, 1243–1249, https://doi.org/10.1016/0016-7037(94)90378-6, 1994.

Boudreau, B. P.: Diagenetic models and their implementation, vol. 505, Springer Berlin, https://doi.org/10.1007/978-3-642-60421-8, 1997.

Boudreau, B. P. and Ruddick, B. R.: On a reactive continuum representation of organic matter diagenesis, American Journal of Science, 291, 507–538, https://doi.org/10.2475/ajs.291.5.507, 1991.

Brown, P. N., Byrne, G. D., and Hindmarsh, A. C.: VODE: A variable-coefficient ODE solver, SIAM Journal on Scientific and Statistical Computing, 10, 1038–1051, https://doi.org/10.1137/0910062, 1989.

Burdige, D. J.: Preservation of organic matter in marine sediments: controls, mechanisms, and an imbalance in sediment organic carbon budgets?, Chemical Reviews, 107, 467–485, https://doi.org/10.1021/cr050347q, 2007.

Crank, J.: The mathematics of diffusion, Clarendon Press, Oxford, 1956.

De Borger, E., Tiano, J., Braeckman, U., Rijnsdorp, A. D., and Soetaert, K.: Impact of bottom trawling on sediment biogeochemistry: a modelling approach, Biogeosciences, 18, 2539–2557, https://doi.org/10.5194/bg-18-2539-2021, 2021.

De Leeuw, J. W. and Largeau, C.: A Review of Macromolecular Organic Compounds That Comprise Living Organisms and Their Role in Kerogen, Coal, and Petroleum Formation, in: Organic Geochemistry: Principles and Applications, edited by Engel, M. H. and Macko, S. A., pp. 23–72, Springer US, https://doi.org/10.1007/978-1-4615-2890-6_2, 1993.

Deleersnijder, E., Campin, J.-M., and Delhez, E. J.: The concept of age in marine modelling: I. Theory and preliminary model results, Journal of Marine Systems, 28, 229–267, https://doi.org/10.1016/S0924-7963(01)00026-4, 2001.

Delhez, É. J. and Deleersnijder, É.: The concept of age in marine modelling: II. Concentration distribution function in the English Channel and the North Sea, Journal of Marine Systems, 31, 279–297, https://doi.org/10.1016/S0924-7963(01)00066-5, 2002.

Fick, A.: Über diffusion, Annalen der Physik, 170, 59–86, https://doi.org/10.1002/andp.18551700105, 1855.

Fourier, J. B. J., Darboux, G., et al.: Théorie analytique de la chaleur, vol. 504, Didot Paris, 1822.

Freitas, F. S., Pika, P. A., Kasten, S., Jørgensen, B. B., Rassmann, J., Rabouille, C., Thomas, S., Sass, H., Pancost, R. D., and Arndt, S.: New insights into large-scale trends of apparent organic matter reactivity in marine sediments and patterns of benthic carbon transformation, Biogeosciences, 18, 4651–4679, https://doi.org/10.5194/bg-18-4651-2021, 2021.

Goldberg, E. D. and Koide, M.: Geochronological studies of deep sea sediments by the ionium/thorium method, Geochimica et Cosmochimica Acta, 26, 417–450, https://doi.org/10.1016/0016-7037(62)90112-6, 1962.

Guinasso, Jr., N. and Schink, D.: Quantitative estimates of biological mixing rates in abyssal sediments, Journal of Geophysical Research, 80, 3032–3043, https://doi.org/10.1029/JC080i021p03032, 1975.

John, V., Angelov, I., Öncül, A., and Thévenin, D.: Techniques for the reconstruction of a distribution from a finite number of its moments, Chemical Engineering Science, 62, 2890–2904, https://doi.org/10.1016/j.ces.2007.02.041, 2007.

Jørgensen, B. B.: A comparison of methods for the quantification of bacterial sulfate reduction in coastal marine sediments: I. Measurement with radiotracer techniques, Geomicrobiology Journal, 1, 11–27, https://doi.org/10.1080/01490457809377721, 1978.

Kuderer, M. J. et al.: How bioturbators perturb the paleo record: From Eulerian to Lagrangian and back., Ph.D. thesis, Utrecht University, https://doi.org/10.33540/1544, 2022.

Meile, C. and Van Cappellen, P.: Particle age distributions and O2 exposure times: timescales in bioturbated sediments, Global Biogeochemical Cycles, 19, https://doi.org/10.1029/2004GB002371, 2005.

Meysman, F. J., Boudreau, B. P., and Middelburg, J. J.: Modeling reactive transport in sediments subject to bioturbation and compaction, Geochimica et Cosmochimica Acta, 69, 3601–3617, https://doi.org/10.1016/j.gca.2005.01.004, 2005.

Meysman, F. J., Middelburg, J. J., and Heip, C. H.: Bioturbation: a fresh look at Darwin's last idea, Trends in Ecology & Evolution, 21, 688–695, https://doi.org/10.1016/j.tree.2006.08.002, 2006.

Middelburg, J. J.: A simple rate model for organic matter decomposition in marine sediments, Geochimica et Cosmochimica acta, 53, 1577–1581, https://doi.org/10.1016/0016-7037(89)90239-1, 1989.

Middelburg, J. J.: Marine carbon biogeochemistry: A primer for earth system scientists, Springer Nature, https://doi.org/10.1007/978-3-030-10822-9, 2019.

Middelburg, J. J., Soetaert, K., and Herman, P. M.: Empirical relationships for use in global diagenetic models, Deep Sea Research Part I: Oceanographic Research Papers, 44, 327–344, https://doi.org/10.1016/S0967-0637(96)00101-X, 1997.

Narasimhan, T. N.: Fourier's heat conduction equation: History, influence, and connections, Reviews of Geophysics, 37, 151–172, https://doi.org/10.1029/1998RG900006, 1999.

R Core Team: R: A Language and Environment for Statistical Computing, R Foundation for Statistical Computing, Vienna, Austria, https://www.R-project.org/, 2022.

Soetaert, K.: rootSolve: Nonlinear root finding, equilibrium and steady-state analysis of ordinary differential equations, r package 1.6, 2009.

Soetaert, K. and Meysman, F.: Reactive transport in aquatic ecosystems: Rapid model prototyping in the open source software R, Environmental Modelling & Software, 32, 49–60, https://doi.org/10.1016/j.envsoft.2011.08.011, 2012.

Soetaert, K., Petzoldt, T., and Setzer, R. W.: Solving Differential Equations in R: Package deSolve, Journal of Statistical Software, 33, 1–25, https://doi.org/10.18637/jss.v033.i09, 2010.

Tromp, T., Van Cappellen, P., and Key, R.: A global model for the early diagenesis of organic carbon and organic phosphorus in marine sediments, Geochimica et Cosmochimica Acta, 59, 1259–1284, https://doi.org/10.1016/0016-7037(95)00042-X, 1995.

Vähätalo, A. V., Aarnos, H., and Mäntyniemi, S.: Biodegradability continuum and biodegradation kinetics of natural organic matter described by the beta distribution, Biogeochemistry, 100, 227–240, https://doi.org/10.1007/s10533-010-9419-4, 2010.

Wang, Y. and Van Cappellen, P.: A multicomponent reactive transport model of early diagenesis: Application to redox cycling in coastal marine sediments, Geochimica et Cosmochimica Acta, 60, 2993–3014, https://doi.org/10.1016/0016-7037(96)00140-8, 1996.

Westrich, J. T. and Berner, R. A.: The role of sedimentary organic matter in bacterial sulfate reduction: The G model tested, Limnology and Oceanography, 29, 236–249, https://doi.org/10.4319/lo.1984.29.2.0236, 1984.

Xu, S., Liu, B., Arndt, S., Kasten, S., and Wu, Z.: Assessing global-scale organic matter reactivity patterns in marine sediments using a lognormal reactive continuum model, Biogeosciences Discussions, 2022, 1–22, https://doi.org/10.5194/bg-2022-228, 2022.

Zonneveld, K. A., Versteegh, G. J., Kasten, S., Eglinton, T. I., Emeis, K.-C., Huguet, C., Koch, B. P., de Lange, G. J., de Leeuw, J. W., Middelburg, J. J., et al.: Selective preservation of organic matter in marine environments; processes and impact on the sedimentary record, Biogeosciences, 7, 483–511, https://doi.org/10.5194/bg-7-483-2010, 2010.